

TABLE OF CONTENTS

	Page
ACKNOWLEDGEMENTS	iii
ABSTRACT (ENGLISH)	iv
ABSTRACT (THAI)	v
LIST OF TABLES	ix
LIST OF FIGURES	x
ABBREVIATIONS AND SYMBOLS	xiv
CHAPTER 1 INTRODUCTION	1
1.1 Overview	1
1.2 Objectives	2
CHAPTER 2 LITERATURE REVIEW	3
2.1 Dental Porcelains	3
2.1.1 Historical perspective	3
2.1.2 Chemical compositions	4
2.1.3 Structures	7
2.1.4 Application in dental field	12
2.2 Leucite	18
2.2.1 Composition and structure	18
2.2.2 Leucite reinforce dental porcelains	21
2.2.3 Phase transformation of leucite reinforce dental porcelains	25
2.2.4 Content and size of leucite reinforce dental porcelains	27
2.3 Zirconia	31
2.3.1 Composition and structure	32

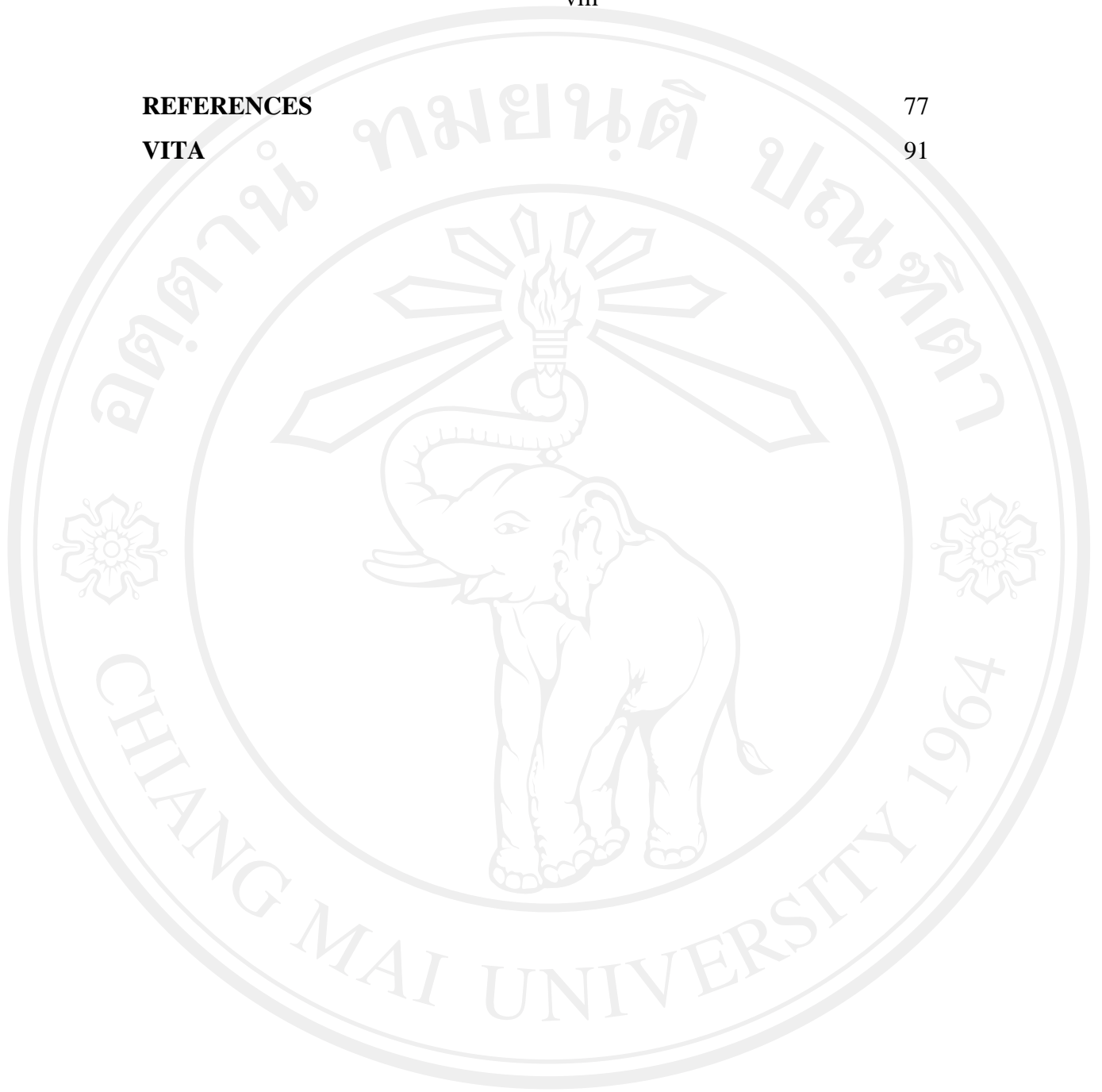
2.3.2 Zirconia reinforced ceramics	32
2.4 Ceramic Nanocomposites	34
2.4.1 Ductile- Phase Toughening	35
2.4.2 Fiber Toughening	35
2.4.3 Transformation Toughening	37
2.4.4 Microcrack Toughening	37
CHAPTER 3 EXPERIMENTAL PROCEDURE	41
3.1 Sample Preparation	41
3.1.1 Powder Preparation	41
3.1.2 Preparation of the specimens	41
3.2 Sample Characterization	47
3.2.1 Density Analysis	47
3.2.2 Phase Analysis	48
3.2.3 Microstructural Analysis	48
3.2.4 Size Analysis	48
3.2.5 Mechanical properties measurement	50
3.2.4.1 Uniaxial Flexural Strength	50
3.2.4.2 Hardness and Elastic Modulus	51
3.2.4.3 Indentation Fracture Toughness	53
3.3 Statistical Analysis	53
CHAPTER 4 RESULTS AND DISCUSSION	56
4.1 Physical properties	56
4.2 Mechanical properties	64
CHAPTER 5 CONCLUSIONS AND SUGGESTIONS FOR FUTURE WORKS	76
5.1 Conclusions	76
5.2 Suggestions for Further Work	76

REFERENCES

77

VITA

91



ลิขสิทธิ์มหาวิทยาลัยเชียงใหม่

Copyright© by Chiang Mai University
All rights reserved

LIST OF TABLES

Table		Page
2.1	Compositions of household and dental porcelains.	5
2.2	Chemical composition analysis of some commercial dental porcelains.	6
3.1	The firing schemes employed for the production of sample.	42
4.1	The firing schemes employed for the production of samples and physical properties.	58
4.2	Average (and standard deviation) of the mechanical properties of ZrO ₂ -reinforced porcelain ceramics.	65
4.3	Results of the Weibull regression analysis of ZrO ₂ -reinforced porcelain ceramics.	72

LIST OF FIGURES

Figure	Page
2.1 Whiteware compositions composed of clay, feldspar, and silica (quartz).	5
2.2 Structural units of SiO_4 tetrahedra: (a) diagram of silicate unit with each SiO tetrahedra sharing an oxygen atom, (b) a silicate unit which the silicon atom (Si) is surrounded by four oxygen atoms (oxygen polyhedra) and (c) linked silicate units which form the network in glass.	8
2.3 Two-dimensional presentation of an oxide M_2O_3 in (a) the crystalline form and (b) the glass form.	8
2.4 Reaction between sodium oxide and silica tetrahedral. The sodium oxide contributes one of the non-bridging oxygen ions which interrupt the continuity of the silica network.	10
2.5 Two-dimensional representation of the structure of sodium silicate glass (The structure is shown in a simplified form since only three of the four oxygen ions surrounding each silicon ion are depicted.)	11
2.6 Aluminium in a silicate network (The structure is shown in a simplified form; the true structure is three-dimensional, the AlO_4 and SiO_4 groups having tetrahedral configurations.). The alkali metal ion (M^+) such sodium maintains electroneutrality.	12
2.7 Applications of dental porcelain-based ceramics: (a) inlay, (b) all ceramic jacket crown and (c) bridge.	13
2.8 Methods of strengthening dental porcelain: (a) enameling of metals, (b) enameling of high strength crystalline ceramics and (c) production of pre-stressed surface layers in dental porcelain via ion-exchange.	14
2.9 In all-ceramic restoration, incidental light is transmitted and partially diffused through. On the other hand, when entering a PFM restoration, light is primarily reflected	17

- 2.10 The unit cell of tetragonal leucite (23°C) viewed parallel to {111}. The potassium atoms (spheres) reside along non-intersecting {111} channels; such channels are interconnected via side channels perpendicular to the main channel axis (shown as *lines* radiating from the central K atoms to neighbouring K atoms in adjacent channels; the distances between such K atoms are approximately 4.7 Å). Directions of the side channels are indexed. 20
- 2.11 View parallel to {110} showing the arrangement of potassium atoms and the six-fold tetrahedral rings along the {111} direction. (a) Below T_C , the potassium atoms (spheres) are off-centered with respect to the channel axis (*diagonal line*). (b) At 800°C, in the cubic phase, the potassium atoms are aligned parallel to the (*triad*) channel axis, and the rings assume an undistorted profile. The average distance between the potassium ions parallel to this axis is approximately 6 Å. 21
- 2.12 Position of feldspathic ceramic bodies for denture teeth and for ceramo-metallic restorations in the ternary-phase diagram $K_2O-Al_2O_3-SiO_2$. Phase diagram reprinted by permission of American Ceramic Society. 22
- 2.13 Micrograph of crystalline phase reinforced porcelains; (a) leucite, (b) lithium disilicate, (c) zirconia, and (d) fluoro-apatite. 24
- 2.14 Schematic of microcracks during cooling of porcelain from the glass transition temperature to room temperature. As the porcelain cools down from the firing temperature, the leucite contracts more than the surrounding glass matrix, owing to its higher coefficient of thermal expansion and the cubic-to-tetragonal phase transformation. At some temperature below the glass transition temperature of the glass matrix, the walls of the cracks around the leucite particles separate due to the contraction of the leucite particles. 26
- 2.15 Schematic representation of the three polymorphs of ZrO_2 : (a) cubic, (b) tetragonal, and (c) monoclinic. 33

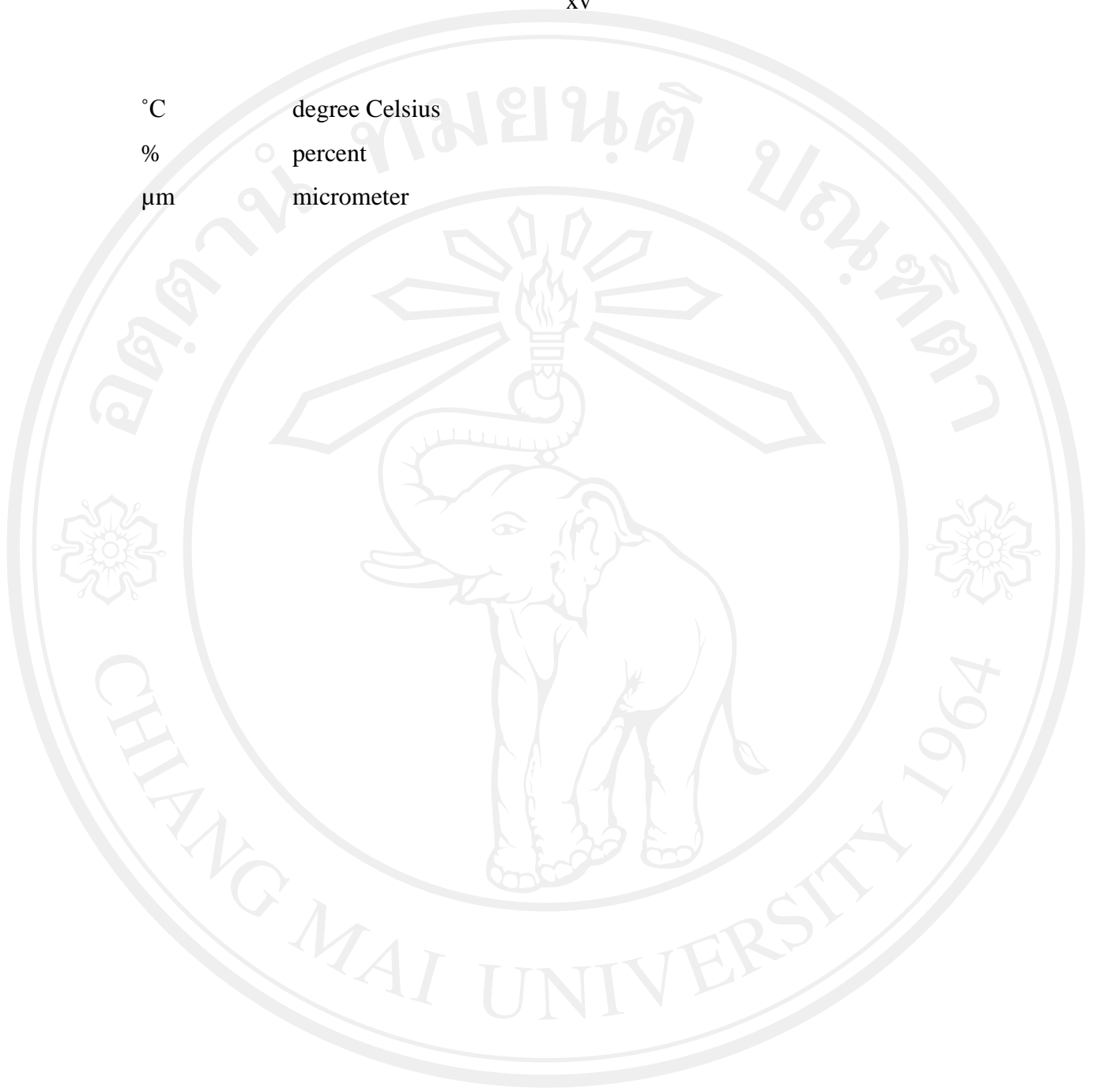
2.16	Schematic illustrations of toughening mechanisms in ceramic-matrix composites: (a) ductile-phase toughening, (b) fiber toughening, (c) transformation toughening, and (d) microcrack toughening.	36
2.17	(a) Niihara's classification of nanocomposite types, based on matrix grain size and second-phase particle size. (b) A new classification, Kuntz in which the matrix phase is continuously nanocrystalline while the second phase varies, leading to four nanocomposite types.	39
3.1	Flow chart of green sample preparations.	43
3.2	Industrial shaping process of dental porcelain by slip casting technique: (1) pouring slip into the metal mold, (2) excess moisture removing, (3) surface flattening, (4) unpacking, (5) green specimen, and (6) sintered specimens.	44
3.3	Vacuum furnace (for reducing sample porosity after sintering process).	45
3.4	Flow chart of the specimen preparations.	46
3.5	Digital scale was used for measuring density by the Archimedes principle.	47
3.6	X-ray diffractometer.	49
3.7	Scanning electron microscope, equipped with EDX analyzer.	49
3.8	Diagram of uniaxial flexural strength test shows rectangular-shaped specimen loaded from above by steel bar and supported from below by adjustable half-round steel plates.	50
3.9	Universal testing machine.	51
3.10	Vickers microhardness testing machine.	52
3.11	Illustration of Vickers indentation and cracks formed around indentation. Dimensions of indentation and cracks to calculate indentation fracture toughness.	52
4.1	X-ray diffraction of patterns of non sintered dental ceramic (a), sintered (b) dental ceramic, non sintered (c) and sintered (d) CG, two-step sintered (e) G3, (f) G4, (g) G5, (h) G6, (i) G7, and (j) G8 samples.	59
4.2	Enlarge X-ray diffraction patterns of (a) G5, (b) G6, (c) G7 and (d) G8 Samples.	60

- 4.3 SEM micrograph of (a) dental porcelain, (b) CG, (c) G5, (d) G6, (e) G7 and (f) G8 samples. 63
- 4.4 Representative (a) SEM micrograph of CG samples and their corresponding EDX analysis, indicating the chemical compositions of (b) glassy matrix, (c) leucite and (d) ZrO_2 phases, respectively. 64
- 4.5 Impression of a Vickers indenter producing symmetric cracks, where the cracks are propagating along the glassy phase of the matrix. The crack patterns are propagating normally to the orientation of the crystalline reinforced phase. 66
- 4.6 SEM micrograph of cracks in the dental porcelain ceramics propagated directly through the glassy phase. 67
- 4.7 Impression of a Vickers indenter producing symmetric cracks, where the cracks are propagating along the glassy phase of the matrix and crystalline reinforced phase. 67
- 4.8 SEM micrograph of (a) and (b) G6; (1) a branch of the intergranular crack is propagating through a glassy phase, (2) transgranular cracking through the grain of crystalline reinforced phase and (3) microcracks are visible in the glassy matrix and at the interface between particles and glass. 68
- 4.9 The comparative hardness data of ZrO_2 -reinforced porcelain ceramics. 69
- 4.10 Weibull plots of uniaxial flexure strength data for ZrO_2 -reinforced porcelain ceramics. 71
- 4.11 The cumulative Weibull plots of probability of failure data for ZrO_2 -reinforced porcelain ceramics. 73
- 4.12 The comparative all flexural strength data of ZrO_2 -reinforced porcelain ceramics. 73
- 4.13 The comparative all fracture toughness data of ZrO_2 -reinforced porcelain ceramics. 75

ABBREVIATIONS AND SYMBOLS

Å	Angstrom
ANOVA	Analysis of Variance
ASTM	American Society for Testing Materials
cm	centimeter
EDX	Energy Dispersive X-ray Spectrometry
g	gram
GPa	gigapascal
g/cm ³	gram per cubic centimeter
ISO	International Organization for Standardization
JCPDS	Joint Committee for Powder Diffraction Standards
λ	Lambda
\ln	Logarithm
K_{IC}	fracture toughness
kV	kilovolt
m	Weibull moduli
mA	miliampare
min	minute
mm	millimeter
mm ³	Cubic Millimeter
MPa	megapascal
N	Newton
nm	nanometer
pm	picometer
PVA	Polyvinyl Alcohol
SEM	Scanning Electron Microscopy
vol%	percent volume
wt%	percent weight
XRD	X-ray Diffraction

°C degree Celsius
% percent
μm micrometer



ลิขสิทธิ์มหาวิทยาลัยเชียงใหม่
Copyright © by Chiang Mai University
All rights reserved